Transactions of the Korean Nuclear Society Autumn Meeting
Changwon, Korea, October 20-21, 2022

Investigation of Impact of Delayed Neutron Data on Dynamic Reactivity

YuGwon Jo*, Hwan-Soo Lee, and Eun-Ki Lee

Korea Hydro & Nuclear Power Co., Ltd. Central Research Institute,
70, Yuseong-daero 1312beon-gil, Yuseong-gu, Daejeon, Korea 34101
**yugwonjo@khnp.co.kr*

1. Introduction

The delayed neutrons are emitted from the beta-decay of neutron-rich fission product nuclei (i.e., delayed neutron precursors), where the half-lives of the delayed neutron precursors ranges from 0.1 seconds to nearly a minute. Although the delayed neutrons comprise around 1% of the total fission neutrons, they are important to maintain the nuclear reactor in the delayed critical state and provide the operator control time.

In 1965, Keepin et al [1] proposed the six-group representation of the delayed neutron data rather than the individual precursor data for the reactor physics analysis. They found that the six-group delayed neutron yields and decay constants optimally fitted the temporal behavior of the experimental data. Due to the accuracy and the computational efficiency of the six-group representation in the reactivity measurement using the inverse point-kinetics, it becomes the industrial standard. There have been many efforts to evaluate and improve the six-group delayed neutron data beyond Refs. [2-7], which are compiled into the standard evaluated nuclear data libraries such as ENDF/B and JENDL. In the meanwhile, the JEFF library adopted an eight-group structure to separate out the dominant longest-lived precursors such as Br-87, I-137, and Br-88. However, Tuttle's recommended six-group delayed neutron data [3-4] is still widely used to estimate reactivity from the reactor kinetic response, even though the data is not up-to-date.

Table I compares the delayed neutron data of major fissionable isotopes (U-235, U-238, and Pu-239) from Tuttle's data, ENDF/B-VII.0 [8], and ENDF/B-VIII.0 [9], where P_i and λ_i indicate the relative abundance and the decay constant [1/sec] for delayed neutron group *i*, respectively. As can be seen in the table, there are some discrepancies in the temporal group data among the libraries, while the differences in total delayed neutron yield ν_d are negligible. For the integral comparison of the temporal delayed neutron data, the delayed neutron mean emission time (T_{avg}) is calculated as $T_{avg} = \sum_{i=1,6} P_i/\lambda_i$ and provided in Table I. Compared to the Tuttle's data, the delayed neutron mean emission times from ENDF/B-VII.0 and ENDF/B-VIII.0 show non-trivial discrepancies.

It should be noted that the delayed neutron data of ENDF/B-VII.0 drastically changed from that of previous ENDF/B-VI.8 by adopting the theoretical model prediction. However, the delayed neutron data since ENDF/B-VII.1 [10] was reverted back to ENDF/B-VI.8 because of issues raised from the reactivity measurements.

This paper investigates the impacts of delayed neutron data on the dynamic reactivity estimated by the inverse point kinetics (IPK) method for a given simulated reactor response and that by the three-dimensional (3-D) nodal kinetics calculation. The numerical results for a typical light water reactor show that the reactivity from the IPK model significantly varies depending on the delayed neutron library, while the reactivity from the 3-D nodal kinetics calculation is almost invariant.

Table I. Comparisons of delayed neutron data of major fissionable isotopes (U-235, U-238, and Pu-239)

Delayed Neutron Data	U-235			U-238			Pu-239		
	Tuttle[1]	E70[2]	E80[3]	Tuttle[1]	E70[2]	E80[3]	Tuttle[1]	E70[2]	E80[3]
P_1	0.0380	0.0130	0.0380	0.0328	0.0142	0.0328	0.0350	0.0139	0.0350
P_2	0.2130	0.1370	0.2800	0.1979	0.1415	0.2874	0.1807	0.1128	0.2980
P_3	0.1880	0.1620	0.2160	0.1799	0.1365	0.1690	0.1725	0.1310	0.2110
P_4	0.4070	0.3880	0.3280	0.3813	0.3722	0.3066	0.3868	0.3851	0.3260
P_5	0.1280	0.2250	0.1030	0.1490	0.2420	0.1606	0.1586	0.2540	0.0860
P_6	0.0260	0.0750	0.0350	0.0591	0.0936	0.0437	0.0664	0.1031	0.0440
λ_1[s^{-1}]	0.0127	0.0125	0.0133	0.0132	0.0125	0.0136	0.0129	0.0125	0.0128
λ_2[s^{-1}]	0.0317	0.0318	0.0327	0.0321	0.0303	0.0313	0.0311	0.0299	0.0301
λ_3[s^{-1}]	0.1150	0.1094	0.1208	0.1390	0.1159	0.1233	0.1340	0.1072	0.1238
λ_4[s^{-1}]	0.3110	0.3170	0.3028	0.3580	0.3415	0.3237	0.3310	0.3176	0.3254
λ_5[s^{-1}]	1.4000	1.3540	0.8495	1.4100	1.3186	0.9060	1.2600	1.3524	1.1220
λ_6[s^{-1}]	3.8700	8.6364	2.8530	4.0200	9.9790	3.0487	3.2100	10.691	2.6970
ν_d	0.01673	0.01670	0.01670	0.04389	0.0444	0.0444	0.0063	0.00645	0.00645
T_{avg}[4][s]	12.75	11.81	11.06	7.68	8.28	7.19	14.64	14.88	15.43
Diff[5][%]	-	-7.41	-13.27	-	7.75	-6.40	-	1.64	5.34

[1]Tuttle's recommended six-group data [3-4]
[2]ENDF/B-VII.0 six-group data [8]
[3]ENDF/B-VIII.0 six-group data (adopted from ENDF/B-VI.8) [9]
[4]Delayed neutron mean emission time [s]
[5]Relative difference [%] of the delayed neutron emission time against Tuttle's data

2. Framework for Sensitivity Analysis

Figure 1 shows the framework for the sensitivity analysis of the dynamic reactivity for various delayed neutron libraries. In this work, the Tuttle's data was considered as a reference library for the sensitivity analysis, while ENDF/B-VII.0 and ENDF/B-VIII.0 were chosen as test libraries.

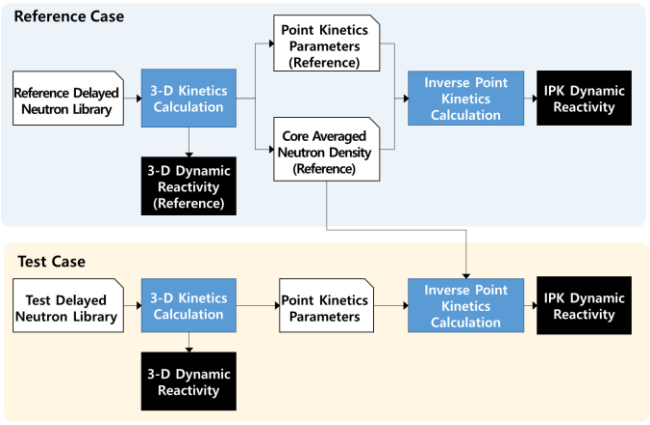

Figure 1. Framework for the sensitivity analysis of the dynamic reactivity for various delayed neutron libraries.

As shown in Figure 1, the 3-D nodal kinetics calculation was performed with each delayed neutron library to evaluate the adjoint-weighted point kinetics parameters and the dynamic reactivity which can be calculated as:

$$\rho_i^{3D} = \sum_{m=1}^{M} V^m \sum_{g=1}^{2} W_g^m \left[\chi_{p,g} \upsilon \Sigma_{f,g,i}^m \phi_{g,i}^m + \sum_{g'=1}^{2} \Sigma_{gg'}^m \phi_{g',i}^m - L_{g,i}^m - \Sigma_{a,g,i}^m \phi_{g,i}^m \right] \Big/ \sum_{m=1}^{M} V^m \sum_{g=1}^{2} W_g^m \chi_{p,g} \upsilon \Sigma_{f,g,i}^m \phi_{g,i}^m, \quad (1)$$

where i is the temporal discretization index, m is the spatial node index, g is the neutron energy group index, V^m is the volume of the spatial node, $L_{g,i}^m$ is the neutron leakage rate, W_g^m is the adjoint flux, and $\phi_{g,i}^m$ is the neutron flux.

In the reference case, the core-averaged neutron density (CAND) was additionally calculated as:

$$n_i^{ref} = \sum_{m=1}^{M} V^m \sum_{g=1}^{2} W_g^m \frac{\phi_{g,i}^m}{v_g^m} \Big/ \sum_{m=1}^{M} V^m \sum_{g=1}^{2} W_g^m, \quad (2)$$

where v_g^m is the average neutron speed for group g.

Then, for each test case, the reference CAND obtained by Eq. (2) was used as an input value for the inverse point kinetics (IPK) calculation to evaluate the IPK reactivity as:

$$\rho_i^{IPK} = \left[\sum_{k=1}^{6} \beta_{k,i} \right]_{beta\ term} + [\Lambda_i \omega_i]_{omega\ term} + \left[-\frac{\Lambda_i}{n_i^{ref}} \sum_{k=1}^{6} \lambda_{k,i} C_{k,i} \right]_{precursor\ term} + \left[-\frac{\Lambda_i}{n_i^{ref}} S_{fixed} \right]_{fixed\ source\ term}, \quad (3)$$

where k is the delayed neutron group index, Λ_i, $\beta_{k,i}$, and $\lambda_{k,i}$ are the point kinetics parameters obtained from the 3-D kinetics calculation, and S_{fixed} is the adjoint-weighted fixed-source term. In Eq. (3), ω_i and $C_{k,i}$ can be calculated respectively as:

$$\omega_i = \frac{1}{\Delta t_i} log \left(\frac{n_i^{ref}}{n_{i-1}^{ref}} \right). \quad (4)$$

$$C_{k,i} = C_{k,i-1} \exp(-\lambda_{k,i} \Delta t_i) + \frac{\beta_{k,i} n_{i-1}^{ref}}{\Lambda_i} \frac{\exp(\omega_i \Delta t_i) - \exp(-\lambda_{k,i} \Delta t_i)}{\omega_i + \lambda_{k,i}}. \quad (5)$$

The reference CAND mimics the ex-core detector measurement or the measured CAND based on an appropriate conversion factor [11],[12] in reality.

3. Numerical Results

The sensitivity analysis was performed on a typical light water reactor problem, where the tested transient scenario was as follows. The reactor was initially critical at the all-rod-out (ARO) condition and a control rod bank was fully inserted at the constant speed for 200 s. The RAST-K v2 [13] was used to perform the 3-D nodal kinetics calculation. Table II compares the adjoint-weighted delayed neutron data calculated at the initial steady-state, while Table III compares the dynamic reactivities at the fully inserted condition calculated by both the 3-D kinetics and the IPK calculations for each delayed neutron library.

From Table II and Table III, the followings are observed:
(1) The delayed neutron mean emission times (T_{avg}) become shorter 3.3% for E70 case and 9.9% for E80 case.
(2) The dynamic reactivity from the 3-D kinetics calculation is insensitive to the delayed neutron library.
(3) The IPK reactivities are reduced 4.4% for E70 case and 13.8% for E80 case, which shows similar trend in T_{avg}.

Table II. Adjoint-weighted delayed neutron data at the initial steady-state (BOC, ARO, HZP, NoXe condition)

Group	Tuttle	E70	E80
β_1	0.00021	0.00018	0.00019
β_2	0.00140	0.00135	0.00122
β_3	0.00119	0.00110	0.00108
β_4	0.00239	0.00225	0.00230
β_5	0.00086	0.00099	0.00102
β_6	0.00019	0.00035	0.00039
λ_1[s^{-1}]	0.01275	0.01251	0.01332
λ_2[s^{-1}]	0.03164	0.03132	0.03213
λ_3[s^{-1}]	0.12011	0.11034	0.12134
λ_4[s^{-1}]	0.32099	0.32128	0.30810
λ_5[s^{-1}]	1.40090	1.32372	0.87314
λ_6[s^{-1}]	3.87005	8.67110	2.90126
β_{total}	0.00623	0.00622	0.00620
Diff. in β_{total}	-	-0.00001	-0.00003
T_{avg} [s]	12.58	12.16	11.33
Diff. in T_{avg} [%]	-	-3.31	-9.89

Table III. Dynamic reactivities at the fully inserted condition calculated by 3-D kinetics and IPK calculations

Delayed Neutron Library	3-D Kinetics Calculation			IPK Calculation		
	ρ^{3D} [pcm]	Diff. [pcm]	Rel. Diff. [%]	ρ^{IPK} [pcm]	Diff. [pcm]	Rel. Diff. [%]
Tuttle	-1138.9	-	-	-1138.9	0.0	0.0
E70	-1139.7	-0.8	0.1	-1088.8	50.1	-4.4
E80	-1140.5	-0.7	0.1	-981.4	158.3	-13.8

Figure 2 shows the IPK reactivity components (see Eq. (2)) for each delayed neutron library, where the precursor terms are dominant for the discrepancies of the IPK reactivity. This explains that the differences in the delayed neutron data flow into those in the IPK reactivities. It is noted that the fixed source term was neglected in this study. On the other hand, as expected, the ρ^{3D} is insensitive to the delayed neutron library due to that the ρ^{3D} is a consequently calculated value based on the 3-D flux and precursor distribution aroused by a control rod moving and the static rod worth is constant. However, the variation of CAND of the three cases are not the same because of the delayed neutron library.

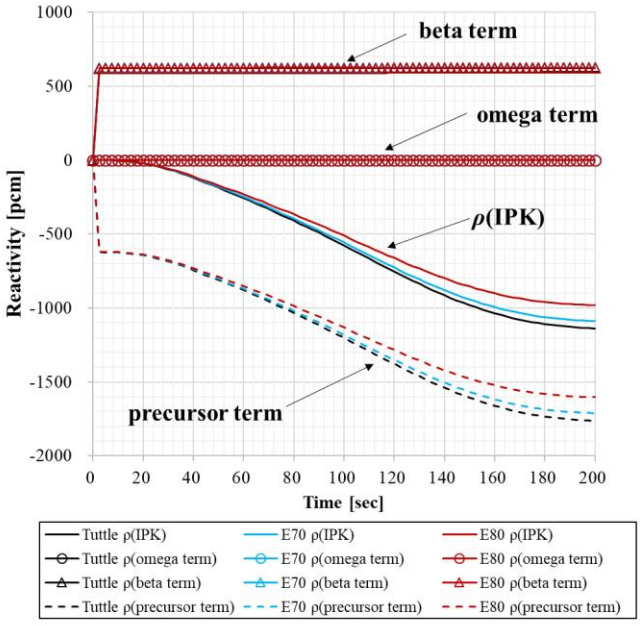

Figure 2. Comparisons of the IPK reactivity components

5. Summary and Conclusions

This paper investigated the impacts of delayed neutron library on the dynamic reactivity estimated by the IPK and the 3-D nodal kinetics calculations. Compared to the traditional Tuttle's data, the IPK reactivities based on ENDF/B-VII.0 and ENDF/B-VIII.0 showed significant differences, while the reactivities from the 3-D nodal kinetics calculation are insensitive. It should be noted that the results shown in this paper are to provide the sensitivity analysis and do not imply the accuracy of the individual delayed neutron library. However, since the delayed neutron data not only affect the reactivity measurement but also affect the safety analysis based on the point-kinetics model, a careful examination is necessary when we update the delayed neutron library.

REFERENCES

[1] G.R. Keepin, et al., "Delayed Neutrons from Fissionable Isotopes of Uranium, Plutonium, and Thorium," J. Nuclear Energy, 6, 1-21 (1957).
[2] S. A. Cox, "Delayed Neutron Data – Review and Evaluation," ANL/NDM-5, April 1974.
[3] R. J. Tuttle, "Delayed-Neutron Data for Reactor Physics Analysis," Nucl. Sci. and Eng., 56, 37-71 (1975).
[4] R. J. Tuttle, "Review of Delayed Neutron Yields and Nuclear Fission," Proc. Consultants' Mtg. on Delayed Neutron Properties, Vienna, Austria, March 26-30, 1979.
[5] M. C. Brady, "Evaluation and Application of Delayed Neutron Precursor Data," PhD Thesis, Texas A&M University (1989).
[6] D.J. Loaiza, et al., "Measurements of absolute delayed neutron yield and group constants in the fast
[7] P. Dimitriou, et al., "Development of a Reference Database for Beta-Delayed Neutron Emission," Nuclear Data Sheets, 173, 144-238 (2021).
[8] M.B. Chadwick, et al., "ENDF/B-VII.0: Nest Generation Evaluated Nuclear Data Library for Nuclear Science and Technology," Nuclear Data Sheets, 107, 2931-3060 (2006).
[9] M.B. Chadwick, et al., "ENDF/B-VIII.0:The 8th Major Release of the Nuclear Reaction Data Library with CIELO-project Cross Sections, New Standards and Thermal Scattering Data," Nuclear Data Sheets, 148, 1-142 (2018).
[10] M.B. Chadwick, et al., "ENDF/B-VII.1 Nuclear Data for Science and Technology: Cross Sections, Covariances, Fission Product Yields and Decay Data," Nuclear Data Sheets, 112, 2887-2996 (2011).
[11] E.K. Lee, et al., "New Dynamic Method to Measure Rod Worths in Zero Power Physics Tests at PWR Startup," Annals of Nuclear Energy, 32, 1457-1475 (2005).
[12] E.K. Lee, et al., "Dynamic Rod Worth Measurement Method Based on Equilibrium-Kinetics Status," Nuclear Eng. Tech., 54, 781-789 (2022)
[13] J. Park, et al., "RAST-K v2 – Three-dimensional Nodal Diffusion for Pressurized Water Reactor Core Analysis," Energies, 13, 6324 (2020).